DESIGN AND ANALYSIS OF INDEPENDENT STRUT TYPE AIR SUSPENSION APPLIED TO HIGH CLEARANCE SELF-PROPELLED SPRAYER
/
应用于高地隙自走式喷雾机的独立式立轴空气悬架设计与分析

Chenwei HU [1)], Jiayu CAO [1)], Shuo ZHANG[1)], Yu CHEN*[1)], Liquan LU [1)]
[1)] Northwest A&F University, Yangling 712100, China;
Tel: +86 17795759790; E-mail: jdxy73@nwafu.edu.cn
DOI: https://doi.org/10.35633/inmateh-71-04

Keywords: *high clearance self-propelled sprayer, air suspension, design, simulation, analysis*

ABSTRACT
As an important plant protection machinery for spraying and fertilizing crops, high clearance self-propelled sprayer is of great significance to promote food security production and stable development of agriculture. Aiming at the complex operating conditions and unique operating requirements of large high clearance self-propelled sprayer, this paper analyzes and determines the main components of the sprayer suspension, such as elastic components, guiding devices, buffer devices, damping components, etc., and designs a stand-alone vertical shaft air suspension system structure suitable for high clearance sprayers. The stress of the sprayer chassis under different extreme conditions such as side slip, emergency braking and uneven road driving is analyzed, and the vertical shaft is designed and checked in detail. Based on the stress analysis results of the sprayer chassis, the finite element analysis software HyperMesh 10.0 was used to analyze the statics of the key components of the suspension, such as the vertical shaft, the motor protection shell, the steering arm, and the spring top support. According to the results of force analysis and finite element analysis, combined with the requirements of process production, the suspension structure in the design scheme is improved, and the final suspension form and the whole structure scheme of the sprayer are obtained. Through this study, it provides a basis for the design and development of large high clearance self-propelled sprayer.

摘要
作为对农作物进行喷药、施肥等作业的重要植保机械，高地隙自走式喷雾机对促进粮食安全生产和农业稳定发展具有非常重要的意义。本文针对大型高地隙自走式喷雾机复杂的运行工况和独特的作业要求，分析确定喷雾机悬架的弹性元件、导向装置、缓冲装置、阻尼元件等主要部件，设计了适用于高地隙喷雾机的独立式立轴空气悬架系统结构方案。分析喷雾机底盘在侧滑、紧急制动、不平路面行驶等不同极限工况下的受力情况，并对立轴进行了详细设计与校核。基于喷雾机底盘受力情况分析结果，应用有限元分析软件 HyperMesh 10.0，对悬架关键零部件立轴、马达保护壳体、转向臂、弹簧顶部支撑等进行了静力学分析。根据受力分析与有限元分析结果，结合工艺生产要求，对设计方案中的悬架结构形式进行改进，得到最终的悬架形式和喷雾机整机结构方案。通过本文研究，为大型高地隙自走式喷雾机设计与研发提供基础。

INTRODUCTION

High clearance self-propelled sprayer is a kind of large and high-end agricultural equipment (*Sánchez-Hermosilla J. et al., 2022; Hu Y. et al., 2022*), which is characterized by high intelligence, wide operation width, high ground clearance and fast driving speed (*Li W. et al., 2022*). At present, the maximum speed of sprayer has reached 60 km/h. The large ground clearance and high driving speed make it necessary to be equipped with a special suspension system to buffer the vibration. On the one hand, the ride comfort of the driver is improved by vibration reduction. On the other hand, the vibration, swing and rotation of the boom are prevented and reduced, so that it is kept at a constant height, so that the spraying is more uniform, and the drift is reduced. During the operation of the sprayer, the sprung mass changes with the change of the amount of Chinese medicine in the medicine box, which requires the suspension to have a wide adaptability. At the same time, due to the complex and changeable field working environment, the suspension also needs to ensure the balance of the frame and the traction of the whole vehicle. In the process of driving on the road, the speed is high, and the suspension is needed to improve the ride comfort and handling stability of the sprayer. Mainstream agricultural machinery enterprises in the world have developed a variety of sprayer chassis suspensions, and formed the following two characteristics in structure and function:

(1) The suspension with helical spring as elastic element has been applied in sprayer (*Press R.U., 2012; Buschena J., 2012*). For example, the four-wheel independent damping system installed on the Patriot series sprayer produced by Case New Holland and the shock absorber and spiral spring damping system installed on the 3WZG-3000 sprayer produced by modern agricultural equipment. The advantage of this suspension form is that the structure is simple, and the semi-active control of the suspension is realized by using the adjustable damping shock absorber. However, because the spiral spring and the shock absorber are mostly in parallel, it is not convenient to realize the body height stability and load balance control of the sprayer due to the small spring stroke and weak load capacity adjustability.

(2) Independent nonlinear spring suspension, especially air suspension has become the mainstream (*Hung T.M., 2022; Jiang X. et al., 2022; Zhou Y. et al., 2022*). The air spring is widely used in foreign sprayers because of its good nonlinear elastic characteristics, large suspension stroke and adjustable load capacity. Sprayer companies such as John Deere (*Carlson B.C. et al., 2011; Wubben T.M. et al., 2007*), AGCO (*Slawson J., 2013; Steffensen C, et al., 2012)*, HAGIE (*Schaffer J.A., 2002; Schaffer J.A., 2002*), and AgriFac (*Blaauw D., 1999; Ehlen V. et al., 2011*) have applied for patents on air suspensions, and their new generation sprayers are also equipped with air suspension systems. For example, the Miller sprayer uses an air suspension system with a vibration reduction stroke of up to 20 inches. The multi-link guiding device ensures that the air spring is only subjected to vertical force. The John Deere 4000 series sprayer and the sprayer independently developed by our team adopt a four-wheel independent vertical air suspension system (*Chen Yu et al., 2021; Yu Chen et al., 2020*). There is a vertical shaft between the hub and the bottom of the airbag. The top of the airbag is fixed on the sleeve connected to the frame through the gantry. When the sprayer passes through the uneven road surface, the wheel squeezes and stretches the air spring to cushion the vibration. The sprayer equipped with independent vertical shaft air suspension has simple structure, high ground clearance, large vibration reduction range, easy track adjustment and four-wheel steering. It has been widely used in the products of well-known sprayer manufacturers such as HAGIE, AGCO and AGRIFAC. However, the independent sprayer chassis air suspension system is not equipped with a damper due to structural and space constraints, and only relies on the tire and spring self-damping and mechanical structure friction damping to attenuate vibration. When the sprayer is running at a higher speed or on poor road conditions, the vibration reduction effect will be affected.

(3) The research of active and semi-active chassis suspension system has been paid more and more attention. In order to better adapt to the complex working conditions of the sprayer, some manufacturers began to actively develop active and semi-active suspension systems (*Chen, Y et al., 2020; Li, W et al., 2018*). For example, John Deere and HAGIE equipped the mechanical body height adjustment system on their R40 series and STS series sprayer suspensions, respectively. The system ensures that the chassis of the sprayer is always stable in a certain height range when the charge ratio of the tank changes, thus ensuring the vibration reduction performance of the suspension and the stability of the body. AGCO is equipped with a hydro-pneumatic suspension system that integrates ground clearance adjustment and wheelbase adjustment on its Challenger RG600 series sprayers (*Hiddema J., 2013; Zatrieb J. et al., 2012)*. A variable orifice is connected between the accumulator and the hydraulic cylinder, and the system damping can be adjusted by changing the size of the orifice. One end of the double-acting hydraulic cylinder in the hydro-pneumatic suspension is connected to the motor shell, and the other end is connected to the frame. Through the expansion of the hydraulic cylinder, the sprayer 's ground clearance can be changed steplessly between 75 cm and 120 cm. At the same time, there are two four-way solenoid valves between the inlet and outlet of the oil cylinder of the left and right hydro-pneumatic suspensions. During normal driving, the solenoid valve is in the left position, the left and right cylinders are not connected, and the hydro-pneumatic suspension is independently supported and damped; when the sprayer rolls seriously, the solenoid valve is in the right position, and the rodless cavity of the left cylinder is connected with rod cavity of the right cylinder. At this time, the roll stiffness increases, which can effectively reduce the roll of the whole machine.

In summary, world-renowned agricultural equipment companies such as AGCO, John Deere, HAGIE, AgriFac, etc. have designed and developed a series of suspension systems with air springs as elastic elements for the operation characteristics of high-clearance sprayers. However, due to structural and space constraints, fewer suspensions are equipped with dampers, and most sprayers rely only on tires and spring damping to attenuate vibration. When the sprayer is running at a higher speed or on poor road conditions, the vibration reduction effect will be greatly affected. Therefore, how to design a large high clearance self-propelled sprayer suspension system that can meet the requirements of high ground clearance, large vibration reduction stroke, convenient four-wheel steering and wheel track adjustment is a problem to be

solved on the basis of combining the existing suspension system according to the characteristics of large high clearance self-propelled sprayer, such as fast driving speed, high working efficiency, and the change of sprung mass with the change of liquid volume (*Wei Z. et al., 2023; Han J. et al., 2022; Rondelli V. et al., 2022*). Based on this, aiming at the complex operating conditions and unique operating characteristics of large high clearance self-propelled sprayer, this paper designs a stand-alone vertical shaft air suspension system suitable for high-clearance sprayers, and selects and analyzes the main components. Through this study, it provides a basis for the design and development of large high clearance self-propelled sprayer.

MATERIALS AND METHODS

Structural element selection and analysis

According to the design condition requirements of the chassis suspension system of the spray, the main components of the suspension such as elastic elements, guiding devices, buffer devices, damping elements and the structural form of the suspension system of the spray are analyzed and determined.

- **Elastic elements**

The air spring is selected as the elastic element of the suspension system of the spray, which can meet the design requirements of the suspension system such as simple structure, large damping travel, automatic height stability, load balancing capacity, sufficient strength and life (*Chen Y. et al., 2020; Chen Y. et al., 2021*).

Membrane air springs have a small effective area change rate, a compact structure and smaller stiffness under the same load carrying capacity, and are widely used in trucks, buses, and agricultural vehicles. When selecting an air spring, ensuring that its design height is within the recommended range can achieve the best service life and vibration damping performance. The pressure p_{10}, stiffness k_0, and bias frequency f_0 of the membrane air spring at the load W_1 and design height can be calculated from Equations (1) to (3).

$$p_{10} = \frac{m_1 p_{20}}{m_2} \tag{1}$$

$$k_0 = p_{10}\frac{\mathrm{d}A_e}{\mathrm{d}x} + n\left(p_{10} + p_a\right)\frac{A_{e0}^{\ 2}}{V_0} \tag{2}$$

$$f_0 = \frac{1}{2\pi}\sqrt{\frac{k_0}{m}} \tag{3}$$

According to the overall design requirements of the high clearance sprayer, the vehicle is fully loaded with a sprung mass of 12,000 kg, that is, the load distributed on each spring is 3,000 kg. Therefore, the selected air spring needs to be able to output no less than 29.4 KN at the design height and within the pressure range of 4~6 bar. Based on the above requirements, the 1T19L-7 diaphragm air spring produced by Firestone is selected. Its design height is 380 mm, and the static data curve of the spring is shown in Fig.1.

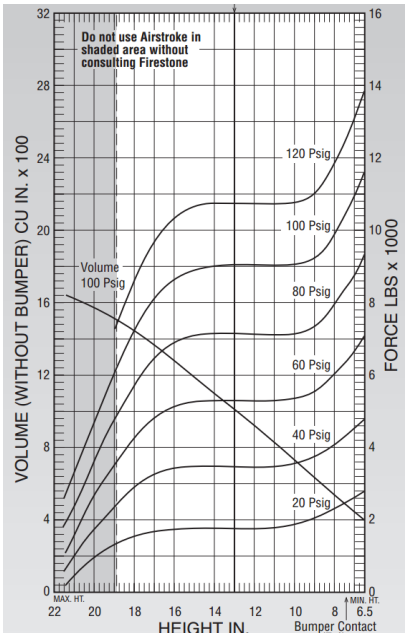

Fig. 1 – Offering of 1T19L-7 reversible sleeve style air spring static data curve by Firestone

By fitting the displacement-load curve and displacement-volume curve under 5 bar in Fig. 1, the effective area and volume formula of the spring are obtained as follows:

$$A_e = \begin{cases} 1.6786(x-0.38)^2 + 0.3761(x-0.38) + 0.0775 & (0.18 \le x \le 0.24) \\ 0.0567 & (0.24 < x < 0.38) \\ -1.4583(x-0.38)^2 - 0.0294(x-0.38) + 0.0565 & (0.38 \le x \le 0.56) \end{cases} \quad (4)$$

$$V = 0.0564(x-0.38) + 0.01914 \quad (0.18 \le x \le 0.56) \quad (5)$$

As described in formulas (4) and (5), the effective area change rate A_e' and volume change rate V_1' of the spring change with the height *h* of the spring, and are less affected by the internal pressure and temperature, which can be ignored. The basic parameters of the spring under the load of 29.4KN and the design height of 380 mm can be calculated from Eqs. (1) to (5), as shown in Tab. 1.

Table 1

Essential parameters of 1T19L-7 reversible sleeve style air spring in 380 mm design height and 29.4 KN load

Load	Gauge pressure	Effective sectional area	Volume	Stiffness	Natural frequency
29.4 KN	5.18 bar	567.5 cm^2	19140 cm^3	163 KN/m	1.17 Hz

- **Buffer device**

The buffer device is mainly to prevent the direct impact between the suspension and the frame, absorb the impact load transmitted from the wheel to the frame, and limit the maximum stroke of the suspension. It can be seen from the static data curve of 1T19L-7 film air spring that the spring height can change in the range of 167~545 mm without buffer device. It is necessary to limit the stroke of air spring in the range of ±100 mm through buffer device to meet the overall design requirements of sprayer. The commonly used buffer device is composed of different materials such as rubber or porous polyurethane. Fig. 2 shows the rubber buffer block structure. The steel plate and rubber are connected by vulcanization, and then the buffer block is fixed and installed on the frame or other parts by the screws on the welded steel plate, which plays the role of limit and protection.

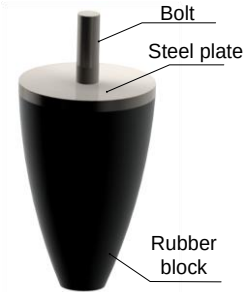

Fig. 2 – Rubber bumper

- **Guiding device**

The guiding device is used to transmit various forces and moments except the vertical force, which determines the motion characteristics of the wheel relative to the frame. In view of the advantages of the McPherson independent suspension system, the structure is appropriately deformed to form an independent vertical shaft suspension system suitable for large high clearance self-propelled sprayer, as shown in Fig. 3.

In Fig. 3(a), the shock absorber in the McPherson independent suspension not only provides damping force, but also supports the body. Its advantage is that the structure is compact and the space is small. The disadvantage is that it cannot bear large lateral force, and additional guide rods such as yaw arm and anti-tilt connecting rod are needed to increase the lateral stiffness and roll stiffness of the suspension. However, the existence of the guide rod system makes it unable to meet the requirements of high clearance of the sprayer. Replace the shock absorber 3 with the vertical shaft 5, remove the guide rod 2, and install the guide shaft 7 on both sides of the spring (to ensure that the spring only bears the vertical force), and obtain the independent vertical shaft suspension system shown in Fig. 3(b). Compared with the McPherson suspension, the ground clearance of the vertical shaft suspension is significantly increased, and the ground clearance can be changed by replacing the vertical shaft with different lengths under the premise of satisfying the stiffness and strength. Since the shock absorber is replaced by the vertical shaft, the vertical shaft suspension needs to be equipped with other forms of damping devices, such as friction dampers or additional air chambers, to attenuate vibration.

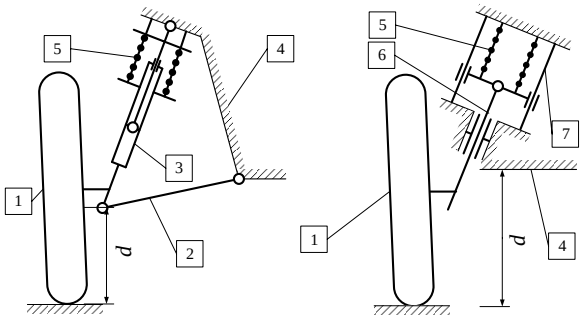

(a) McPherson suspension structure *(b) Independent strut type air suspension structure*

Fig. 3 – Structural sketch of suspension

1. Wheel; 2. Track arm; 3. Shock absorber; 4. Frame; 5. Spring; 6. Strut; 7. Guide shaft; d. Clearance value

- **Damping elements**

A suitable damping device is very important to improve the ride comfort performance of the sprayer. In this paper, according to the structure of the independent vertical shaft air suspension, the additional air chamber air damping suitable for the sprayer suspension is designed. Compared with other damping, the air damping generated by the gas exchange between the air spring and the auxiliary chamber (*Giuseppe Quaglia et al., 2001; Zheng Y et al., 2022; Zheng Y et al., 2023*) has the advantages of less heating, better vibration isolation effect in the frequency band (4~8Hz) which is most sensitive to low frequency and high amplitude vibration and human body. Based on the air spring, an additional air chamber is added, and a throttle valve hole is set between the main and auxiliary air chambers. Throttle valve is a key component to realize air damping, which can adjust the gas mass flow between the spring and the auxiliary chamber. When the air flows through the throttle valve hole A_k from the cross section A_1, the pressure difference ($p_1 \neq p_2$) will be generated at both ends of the throttle valve, which will cause the air to generate damping when passing through the throttle valve (see Fig. 4). By adjusting the aperture size of the throttle valve hole to change the damping of the suspension, the semi-active control of the damping of the sprayer suspension system is realized. In addition, since the arrangement of the additional chamber is not limited by the structure and space, the additional chamber can be placed at any position of the chassis.

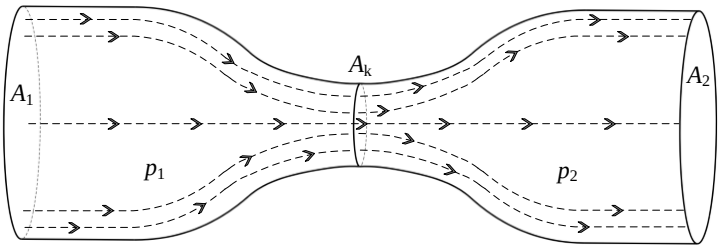

Fig. 4 – Schematic diagram of air flowing through the throttle orifice

Structural design

Based on the McPherson independent suspension, this study designed an independent vertical air suspension system suitable for large high clearance self-propelled sprayer through appropriate deformation and air damping principle.

Fig. 5 shows the preliminary design of the independent vertical air suspension structure assembly based on air damping. Among them, 1~5 form tire assembly T, 7 and 9 form frame connection assembly F, 8, 13 and 15 form steering assembly Z, 10~12, 14~21 and 6 form suspension damping assembly S; the same as Fig. 2-7, the elastic element uses the 1T19L-7 air spring produced by Firestone, and the damping range is about ±100 mm by the internal buffer block and the limit block 16 of the spring. Throttle valve 18 is an important part of air damping device. It can use the gas-specific electromagnetic proportional flow control valve designed and manufactured by iQValves company. It has the advantages of low hysteresis, high frequency response, high pressure resistance and long life.

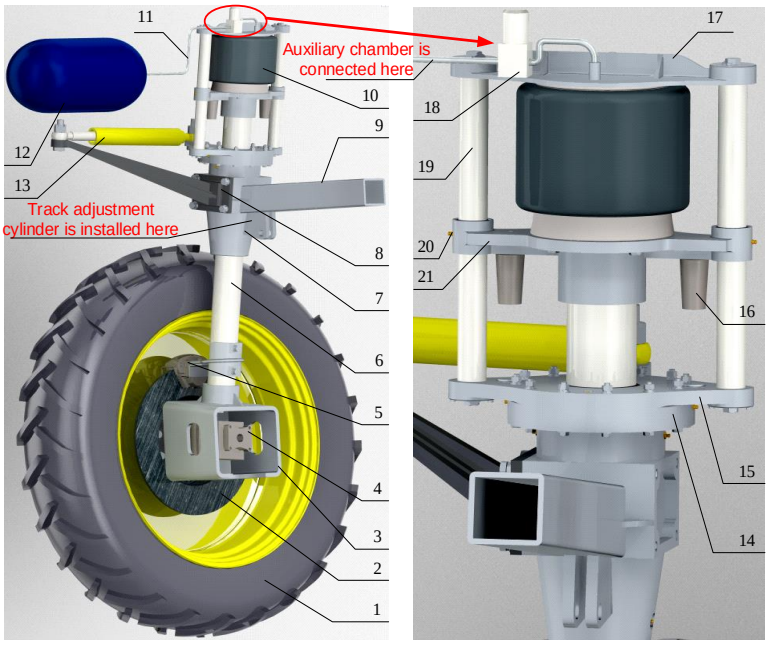

(a) Overall structure *(b) Local large map*

Fig. 5 – Instruction diagram of independent strut type air suspension system based on air damper

1. Wheel; 2. Brake disc; 3. Motor protection housing; 4. Hydraulic motor; 5. Brake caliper installation; 6. Strut; 7. Beam support column; 8. Steering cylinder support arm; 9. Beam; 10. Air spring; 11. Compressed air hose; 12. Auxiliary chamber; 13. Steering cylinder; 14. Positioning ring; 15. Steering arm; 16. Rubber limit block; 17. Spring top support; 18. Variable throttle valve; 19. Guide post; 20. Lubrication mouth; 21. Spring bottom support

Sprayer chassis force analysis

The working conditions of the sprayer are complex. During the operation of the whole machine, it is necessary to bear the effects of vertical, longitudinal, lateral and other forces. Through the force analysis of different extreme conditions (side slip, emergency braking, uneven road driving) of the sprayer chassis, the main structural parameters of the key components are obtained. For the convenience of analysis, it is assumed that the centroid G of the sprayer is located at the center of the whole machine, that is, in the transverse direction, the centroid distance is equal to the distance between the left and right wheels; longitudinally, the distance from the front and rear bridges is equal. On this basis, the following variables and positions are defined: G_m is the full load half vehicle weight, N; GB_1 and GB_2 are the reaction forces on the left and right wheels of the front axle when driving on uneven roads, N; GC_1 and GC_2 are the reaction forces on the left and right wheels of the front axle during sideslip, N; GZ_1 and GZ_2 are the ground reaction forces on the left wheels of the front and rear axles during braking, N; GX_1 and GX_2 are the ground reaction forces on the left wheels of the front and rear axles during climbing, N; FC_1 and FC_2 are the lateral forces on the left and right wheels of the front axle during sideslip, N; FZ_1 and FZ_2 are the braking force of the left wheel of the front and rear axle respectively, N; F_b is the additional load transferred by the braking inertia force, N; F_c is the additional load transferred by sideslip centrifugal force, N; a and b are the distances from the top and bottom joints of the vertical shaft to the axle joints, m; r is the tire rolling radius, m; l is the distance between the axle joint (point O) and the center surface of the tire, m; h is the height of mass center, m; c is the wheel track, m; L is the wheelbase, m; d is the distance from the center surface of the tire to the center surface (O_2 point) of the mounting shaft sleeve, m; w is the length of the axle, m; s is the distance from the contact point under the vertical shaft to the cross section of the tire, m; β is the vertical axis inclination, 8°; θ is the slope angle, 12°; δ is the dynamic load coefficient when passing through the uneven road surface, generally taking 2.5; φ is the peak adhesion coefficient between tire and ground, take 0.7; φ' is the lateral peak adhesion coefficient, take 0.7; G is the center of mass, O_L and O_R are the intersections of the left wheel and the right wheel with the ground, O_F and O_B are the intersections of the front and rear axle center lines with the ground, O is the intersection of the front axle housing support and the left vertical shaft, O_2 and O_3 are the intersections of the vertical shaft with the ground clearance adjustment mechanism and the bottom support of the air spring.

When the sprayer passes through the uneven road surface, the wheels mainly bear the dynamic load. Currently,

$$G_{B1} = G_{B2} = \delta \frac{G_m}{2} \tag{6}$$

When turning, the wheel should bear the lateral force generated by the sprayer (see Fig. 6). When the sideslip occurs, the lateral force reaches the maximum.

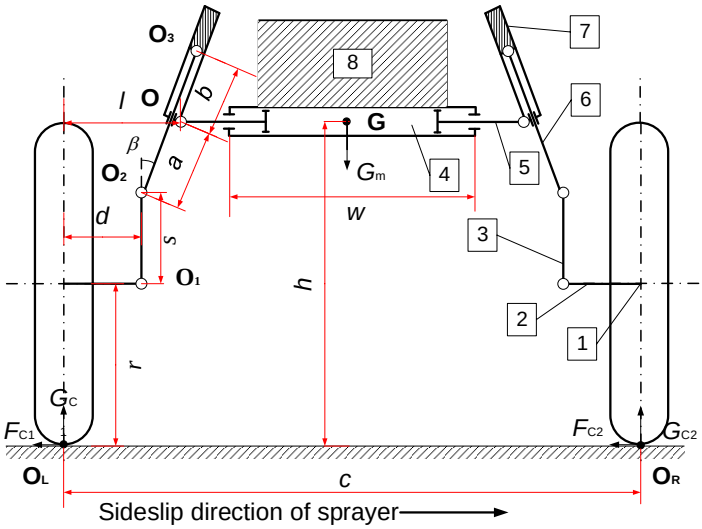

Fig. 6 – Stress analysis diagram of sprayer passing through uneven road and skidding

1. Wheel; 2. Motor; 3. Motor protection housing welding; 4. Axle; 5. Beam; 6. Strut; 7. Air spring; 8. Sprayer body;

Assuming that the sprayer slides to the left side, the left wheel is subjected to the combined action of the vertical load G_L and the additional load F_c transferred by the side slip centrifugal force. Taking the moment of the centroid G in Fig. 6, it can be obtained:

$$G_{C1}\frac{c}{2} = G_{C2}\frac{c}{2} + F_{C1}h + F_{C2}h \tag{7}$$

due to

$$F_{C1} = \varphi' G_{C1} \tag{8}$$

$$F_{C2} = \varphi' G_{C2} \tag{9}$$

$$G_{C1} = \frac{G_m}{2} + F_c \tag{10}$$

$$G_{C2} = \frac{G_m}{2} - F_c \tag{11}$$

The formula (2-8)~(2-11) into formula (2-7), the following is obtained:

$$F_c = \frac{h}{c}\varphi' G_m \tag{12}$$

Then:

$$G_{C1} = (\frac{1}{2} + \frac{h}{c}\varphi')G_m \tag{13}$$

$$G_{C2} = (\frac{1}{2} - \frac{h}{c}\varphi')G_m \tag{14}$$

When the sprayer brakes urgently, the front axle is subjected to the combined action of vertical load G_m and braking inertia force F_b, as shown in Fig. 7.

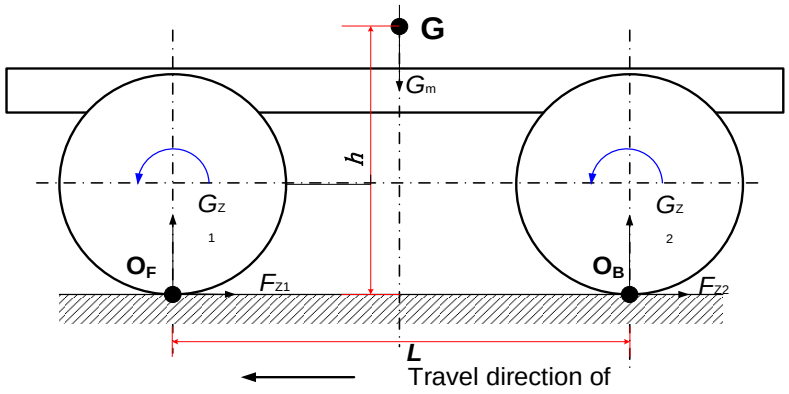

Fig. 7 – Stress analysis diagram of sprayer emergency braking

During the braking process, under the action of negative acceleration, the vertical load is transferred to the front axle. At this time, the moment of the centroid G in Fig. 7 is taken, then:

$$G_{Z1}\frac{L}{2} = G_{Z2}\frac{L}{2} + F_{Z1}h + F_{Z2}h \tag{15}$$

due to

$$F_{Z1} = \varphi G_{Z1} \tag{16}$$

$$F_{Z2} = \varphi G_{Z2} \tag{17}$$

$$G_{Z1} = \frac{G_m}{2} + F_b \tag{18}$$

$$G_{Z2} = \frac{G_m}{2} - F_b \tag{19}$$

The formula (15)~(19) can be obtained:

$$G_{Z1} = \left(\frac{1}{2} + \frac{\varphi h}{L}\right)G_m \tag{20}$$

$$G_{Z2} = \left(\frac{1}{2} - \frac{\varphi h}{L}\right)G_m \tag{21}$$

When the sprayer is climbing, part of the mass of the vehicle will transfer to the rear axle, as shown in Fig. 8. The moments of O_F and O_B are taken respectively, and the reaction force of the left wheel of the front and rear axles can be obtained as shown in Formulas (22) and (23). where θ is the slope angle, rad.

$$G_{X1} = \left(\frac{\cos\theta}{2} - \frac{h}{L}\sin\theta\right)G_m \tag{22}$$

$$G_{X2} = \left(\frac{\cos\theta}{2} + \frac{h}{L}\sin\theta\right)G_m \tag{23}$$

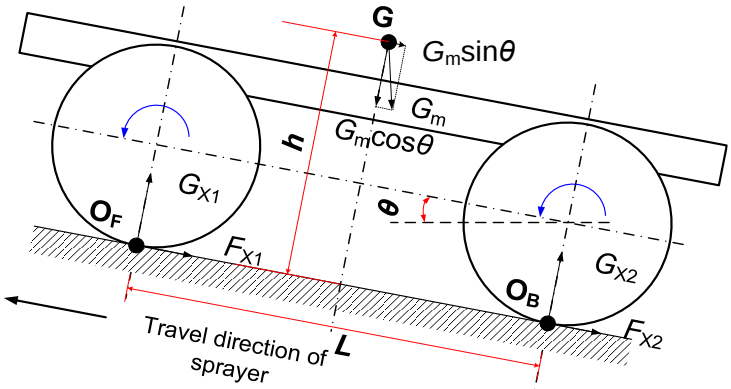

Fig. 8 – Stress analysis diagram of sprayer running on the slope

The following takes the vertical shaft as an example to analyze its stress under different working conditions. In order to simplify the analysis, the backward inclination of the vertical shaft and the camber of the tire are not considered, and it is assumed that the action point of the force is located at the midpoint O_3

and O_2 of the connection between the upper and lower ends of the vertical shaft and the bottom support of the air spring and the support plate on the motor protection shell.

When passing through uneven pavement, the vertical shaft bears dynamic load. Suppose that the forces acting on O_2 and O_3 are F_{BD} and F_{BU}, respectively. According to the moment balance, the moments of O_2 and O_3 are taken respectively.

$$F_{BU} = \delta \frac{G_m}{2} \frac{(l - a\sin\beta)}{a+b} \tag{24}$$

$$F_{BD} = \delta \frac{G_m}{2} \frac{(l + b\sin\beta)}{a+b} \tag{25}$$

When climbing, the forces acting on O_2 and O_3 are set to F_{XD} and F_{XU}, respectively.

$$F_{XU} = \left(\frac{\cos a}{2} + \frac{h}{L}\sin a\right)\frac{(l - a\sin\beta)}{a+b} G_m \tag{26}$$

$$F_{XD} = \left(\frac{\cos a}{2} + \frac{h}{L}\sin a\right)\frac{(l + b\sin\beta)}{a+b} G_m \tag{27}$$

The force analysis of the vertical shaft is shown in Fig. 9. The supporting force G_{C1} generates two opposite forces on the vertical axis, which are F_{CU} and F_{CD} respectively. According to the moment balance, the moments of O_2 and O_3 are taken respectively. From the moment balance, it can be obtained that:

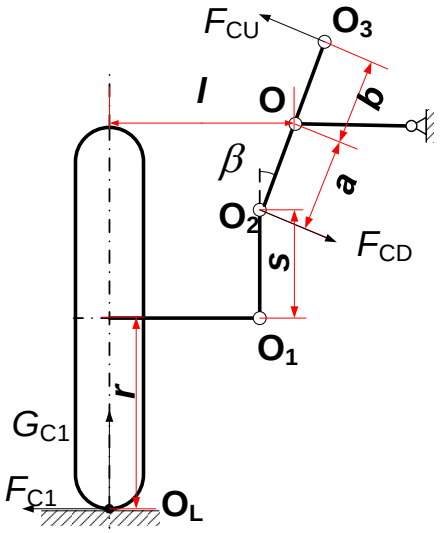

Fig. 9 – Stress analysis schematic diagram of strut under sideslip working condition

$$F_{CU}(a+b) = G_{C1}(l - a\sin\beta) + F_{C1}(r+s) \tag{28}$$

$$F_{CD}(a+b) = G_{C1}(l + b\sin\beta) + F_{C1}(r+s) \tag{29}$$

Bring (8), (13) into (26) and (27):

$$F_{CU} = \frac{(l - a\sin\beta + \varphi' r + \varphi' s)}{2c(a+b)}(c + 2h\varphi')G_m \tag{30}$$

$$F_{CD} = \frac{(l + b\sin\beta + \varphi' r + \varphi' s)}{2c(a+b)}(c + 2h\varphi')G_m \tag{31}$$

Fig. 10 shows the force analysis diagram of the vertical shaft during braking. The supporting force G_{Z1} generates two opposite forces on the vertical shaft, which are F_{ZU1} and F_{ZD1}, respectively.

The braking force F_{Z1} generates two co-directional forces F_{ZU2} and F_{ZD2} on the vertical shaft support. In addition, under the action of braking force F_{Z1}, the axle housing support on the wheel has a tendency to rotate around the vertical axis, which is stopped by the steering cylinder on the steering arm.

At this time, the thrust F_u acting on the steering arm by the steering cylinder produces two co-directional forces F_{ZU3} and F_{ZD3} on the vertical axis support.

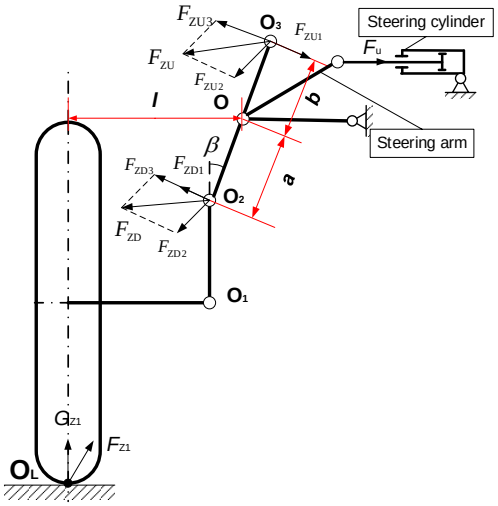

Fig. 10 – Stress analysis schematic diagram of strut under emergency braking working condition.

During braking, the support force G_{Z1} generates two opposite forces on the left front vertical shaft, which are F_{ZU1} and F_{ZD1} respectively. According to the vertical shaft torque balance relationship, it is obtained that:

$$F_{ZU1} = G_{Z1}\frac{(l - a\sin\beta)}{(a+b)} \tag{32}$$

$$F_{ZD1} = G_{Z1}\frac{(l + b\sin\beta)}{(a+b)} \tag{33}$$

The braking force F_{Z1} generates two co-directional forces F_{ZU2} and F_{ZD2} on the vertical shaft support, which are balanced with the thrust F_u acting on the steering arm by the steering cylinder.

$$F_u = \frac{F_{Z1}l}{2\,l'} \tag{34}$$

The two forces F_{ZU2} and F_{ZD2} of F_u on the vertical shaft support are:

$$F_{ZU2} = \frac{F_{Z1}l}{2\,l'}\frac{a}{a+b} \tag{35}$$

$$F_{ZD2} = \frac{F_{Z1}l}{2\,l'}\frac{b}{a+b} \tag{36}$$

The thrust of the steering cylinder acting on the steering arm F_u produces two co-directional forces F_{ZU2} and F_{ZD2} on the vertical shaft:

$$F_{ZU3} = \frac{F_{Z1}l}{2\,l'}\frac{l'' - b\sin\beta}{a+b} \tag{37}$$

$$F_{ZD3} = \frac{F_{Z1}l}{2\,l'}\frac{l'' + a\sin\beta}{a+b} \tag{38}$$

From Fig. 10:

$$F_{ZU} = \sqrt{\left(F_{ZU1} - F_{ZU3}\right)^2 + F_{ZU2}{}^2} \tag{39}$$

$$F_{ZD} = \sqrt{\left(F_{ZD1} + F_{ZD3}\right)^2 + F_{ZD2}{}^2} \tag{40}$$

In the formula, l' is the radius of the steering arm of the sprayer, and l'' is the distance from the end point of the steering arm to O_2.

Bring Eqs. (16), (20), (32)-(38) into Eqs. (39) and (40), the following is obtained:

$$F_{ZU} = \frac{L + 2\varphi h}{4l'L(a+b)}G_m\sqrt{\left(2\,l'\left(l - a\sin\beta\right) - l\varphi\left(l'' - b\sin\beta\right)\right)^2 + \left(la\varphi\right)^2} \tag{41}$$

$$F_{ZD} = \frac{L + 2\varphi h}{4l'L(a+b)}G_m\sqrt{\left(2\,l'\left(l + b\sin\beta\right) + l\varphi\left(l'' + a\sin\beta\right)\right)^2 + \left(lb\varphi\right)^2} \tag{42}$$

From the formula (24)~(27),(30),(31),(41),(42), it can be seen that the force on the lower end of the vertical shaft is greater than that on the upper end.

Therefore, the maximum value in F_{BD}, F_{XD}, F_{CD} and F_{ZD} is taken as the calculation load F_{max} of the vertical shaft. The bending stress, shear stress and extrusion stress of the vertical shaft are calculated as follows:

$$\begin{cases} \sigma_F = \dfrac{32e}{\pi d^3} F_{max} \\ \tau_T = \dfrac{4}{\pi d^2} F_{max} \\ \sigma_C = \dfrac{F_{max}}{de} \end{cases} \quad (2\text{-}43)$$

where e is the contact length between the vertical shaft and the upper and lower connectors, m.

According to the force analysis results of the vertical shaft, combined with the force diagram of the sprayer suspension in Figs. 6~10 and the relationship between the force and the reaction force, the force of other main components of the suspension is obtained, which provides the necessary basis for further finite element analysis and structural improvement of the components.

Finite element analysis of main parts

Compared with other CAE analysis software, HyperMesh has the advantages of high-performance finite element preprocessor and postprocessor, and has a good interface with a variety of CAD software. It can accurately and quickly establish finite element and finite difference models of various complex models, and has been widely used in many manufacturing enterprises and scientific research institutes around the world. In this paper, HyperMesh 10.0 software is used to analyze the key components of the designed independent vertical shaft air suspension system, including spring top support, vertical shaft, motor protection shell and steering arm. Combined with the results of mechanical analysis, the suspension system structure is improved design.

Open HyperMesh 10.0, set the working path, and save the 3D model format as *.stp. In order to ensure the success of HyperMesh 10.0 meshing, the model needs to be simplified in Creo. The simplified parts are mainly chamfering, chamfering and small holes. By meshing, the finite element model is established, and the parameters such as density, elastic modulus and Poisson 's ratio of the model material are set. The stress and strain state of each component is analyzed by adding constraints to the stress analysis results of each component. The parameters of the key components of the designed vertical air suspension are shown in Tab. 2.

Table 2

Material property parameters of key suspension components

Part name	Material	Density (g/cm^3)	Elastic modulus (GPa)	Poisson's ratio
Strut	45	7.85	210	0.31
Motor protection housing	Q345	7.89	135	0.269
Steering arm	Q345	7.89	135	0.269
Spring top support	Q345	7.89	135	0.269

RESULTS AND DISCUSSION

Key parts force analysis results and discussion

Based on the structural size of the whole machine, the variable values shown in Tab. 3 are taken, and the known quantities are brought into Section 2.4 to obtain the chassis force under different working conditions as shown in Tab. 3. The meaning of each symbol in Tab. 3 is known from Section 2.4. According to Tab. 3, the chassis force is closely related to the size of the wheelbase, and increasing the wheelbase can reduce the force of some parts. And the relationship between the size of the force is F_{CD}>F_{ZD}>F_{BD}>F_{XD}, select F_{max}=F_{CD}, according to Formula (2-43), known 45 steel allowable bending stress σ_F=120 MPa, allowable shear stress τ_T=30 MPa, allowable extrusion stress σ_C=50 MPa, check the vertical shaft diameter D≥106 mm. Considering that the selection of some parameters in the preliminary design is not necessarily consistent with the actual situation, some of the limit conditions may not be taken into account. At the same time, the influence of the keyway and cone surface on the spindle is calculated, and the minimum diameter of the vertical shaft is 120 mm. According to the relationship between the force and the reaction force, the force of the motor protection shell is calculated to be 85750 N. The force on the bottom of the steering arm is 34300 N, and the thrust of the steering cylinder is 40004 N; The reaction force of the spring top support is 57291 N. The direction and position of the force are shown in Fig. 11.

Table 3

Mechanical analysis and calculation results of chassis

Known variables		Calculation results		
Variables / measure unit	**Value**	**Force symbol / measure unit**	**When the wheel track is 3.0 m**	**When the wheel track is 3.8 m**
G_m / N	68600	Uneven road excitation condition		
G_b / N	58800	G_{B1} / N	85750	85750
a / m	0.45	G_{B2} / N	85750	85750
b / m	1.05	Sideslip condition		
r / m	0.93	G_{C1} / N	74316.7	65892.1
l / m	0.3	F_{C1} / N	52021.7	46124.5
h / m	2.5	Emergency braking condition		
c / m	3.0~3.8	G_{Z1} / N	74793.1	74793.1
L / m	3.6	F_{Z1} / N	63574.1	63574.1
S / m	0.24	Ramp driving condition		
w / m	1.8	G_{X1} / N	43455.1	43455.1
β / °	8	F_{X1} / N	36936.9	36936.9
Θ / °	12	Stress results of strut		
δ	2.5	F_{BU} / N	13569.8	13569.8
ψ	0.85	F_{BD} / N	25503.9	25503.9
ψ'	0.7	F_{XU} / N	6876.7	6876.7
g / m·s^{-2}	9.8	F_{XD} / N	12924.5	12924.5
l' / m	0.23	F_{CU} / N	52337.4	46404.4
l'' / m	1.3	F_{CD} / N	66256.1	58745.3
B / m	0.38	F_{ZU} / N	23601.7	23601.7
e / m	0.078	F_{ZD} / N	61482.2	61482.2

Simulation results and discussion

The mesh size is defined as 10 mm, and the tetrahedral method is used for meshing. According to the force analysis results of Tab. 3 and the material properties of Tab. 2, the constraints and loads are applied to the parts, and the finite element analysis model of the key parts is obtained as shown in Fig. 11.

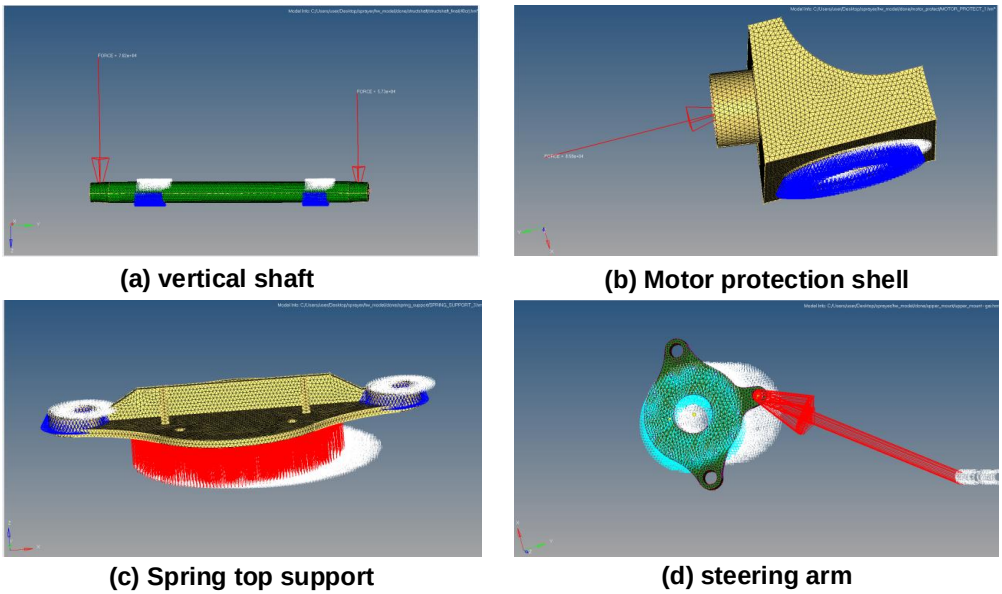

(a) vertical shaft **(b) Motor protection shell**

(c) Spring top support **(d) steering arm**

Fig. 11 – Finite element analytical model of suspension key components

According to the finite element model of the vertical shaft, the stress and strain analysis of the vertical shaft is shown in Fig. 12.

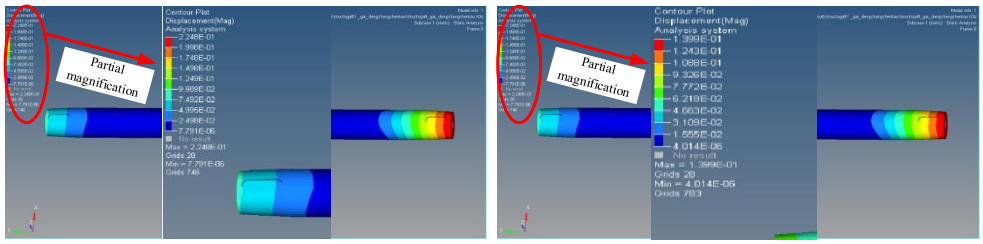

(a) Deformation nephogram of vertical shaft under raw material and structure

(b) Improved vertical shaft axis deformation nephogram

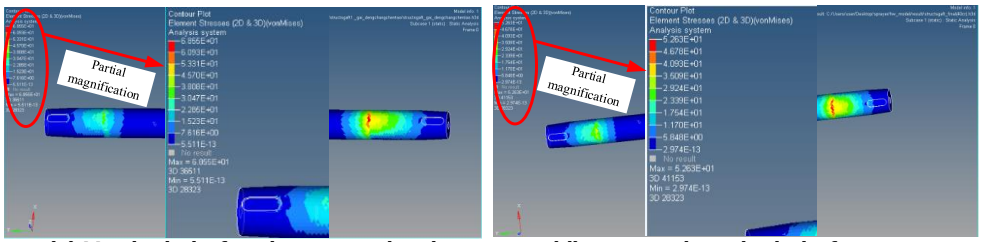

(c) Vertical shaft axis stress cloud diagram of raw materials and structure

(d) mproved vertical shaft stress nephogram

Fig. 12 – Stress and strain nephogram of strut before and after improvement

Fig. 12 (a) and (c) are shown as the stress-strain cloud diagram under the premise that the vertical shaft material is 45 steel, the outer diameter is 100 mm, and the inner diameter is 60 mm. The maximum deformation and stress are 0.224 mm and 68.666 MPa, respectively, which does not meet the allowable stress requirements of the selected material. The outer diameter of the vertical shaft is 120 mm, the inner diameter is 60 mm, and the length of the beam support column is 100 mm. The maximum deformation and stress are 0.1399 mm and 52.6 MPa, respectively, as shown in Fig. 12(b) and (d), which meet the allowable requirements. The improved vertical shaft size by simulation is consistent with the vertical shaft size of the mechanical check, indicating the effectiveness of the mechanical analysis and the accuracy of the simulation structure. Similarly, the finite element analysis of the spring top support, motor protection shell and steering arm is carried out, and the final stress and strain cloud diagram is shown in Fig. 13. The maximum deformation of each part is 1.597 mm, 0.05178 mm and 0.5091 mm respectively, and the maximum stress is 105.2 MPa, 107.5 MPa and 137 MPa respectively. The maximum deformation of the top support of the spring is too large, and the deformation displacement can be reduced by increasing the welding reinforcement. In addition, the maximum stress of each part is too large, which exceeds the allowable stress requirement of Q345, but these maximum values are located at the corners and sharp corners, and stress concentration occurs. Therefore, in the actual machining process, these corners and sharp corners need to be chamfered to eliminate stress concentration.

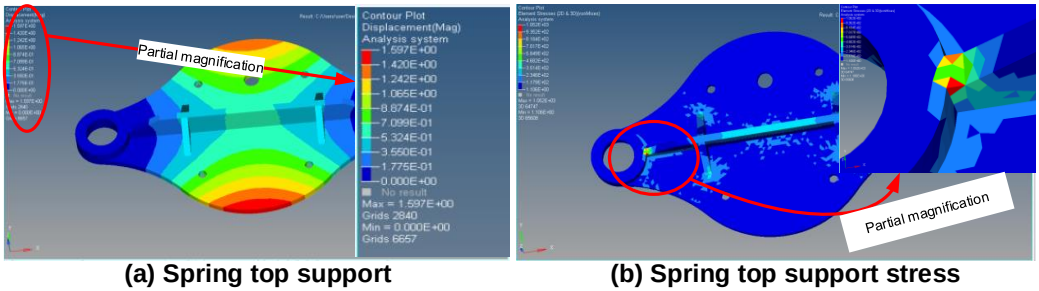

(a) Spring top support deformation nephogram

(b) Spring top support stress nephogram

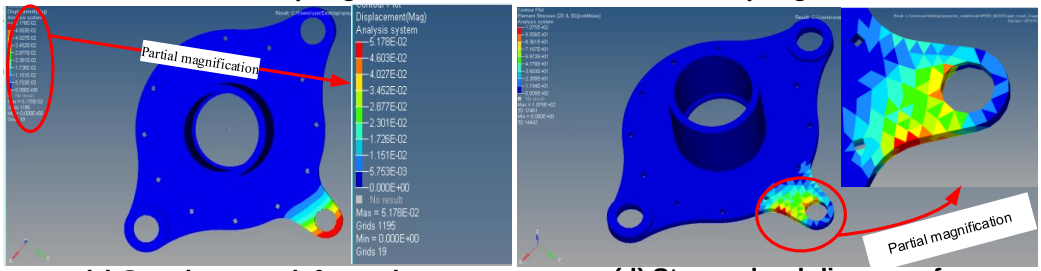

(c) Steering arm deformation nephogram

(d) Stress cloud diagram of steering arm

(e) Deformation cloud diagram of motor protection shell **(f) Motor protection shell stress nephogram**

Fig. 13 – Stress and strain nephogram of suspension key components

According to the finite element analysis method of the key parts of the suspension, the finite element model of the remaining parts is established. According to the results of the finite element analysis, the final structure of the suspension is improved.

Analysis of the final structure of the sprayer

According to the results of force analysis and finite element analysis, combined with the requirements of process production, the suspension structure in the design scheme is improved, and the final suspension structure is obtained as shown in Fig. 14.

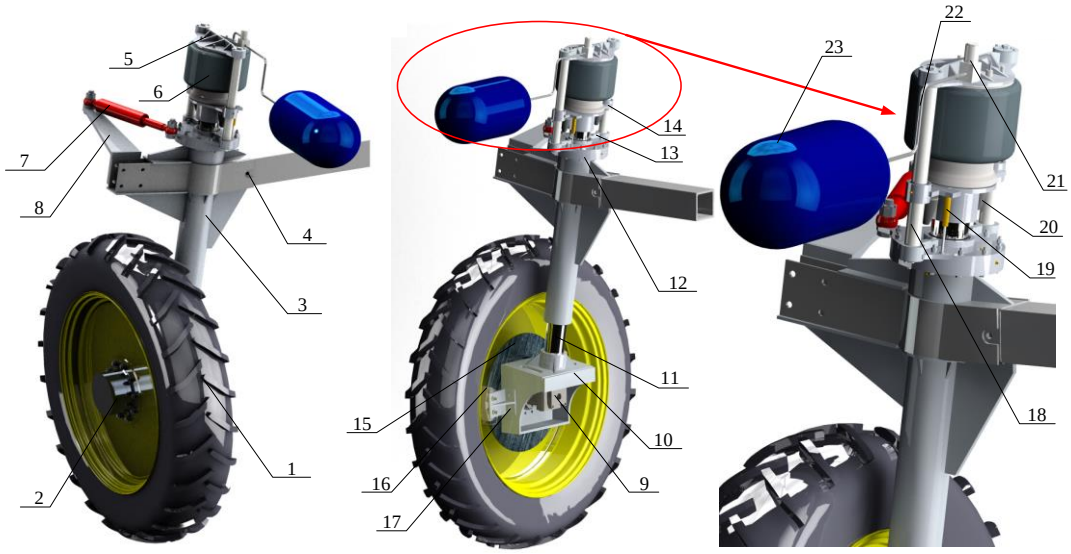

(a) Exterior view *(b) Inner view* *(c) Partial magnification*

Fig. 14 – Final structure form of independent strut type air suspension system

1. Wheel; 2. Reducer; 3. Beam support column; 4. Track adjustment cylinder mounting hole; 5. Spring top support; 6. Air spring; 7. Steer cylinder; 8. Steer cylinder support arm; 9. Hydraulic motor; 10. Motor protection housing; 11. Strut; 12. Positioning ring; 13. Steering arm; 14. Spring bottom support; 15. Brake disc; 16. Brake caliper; 17. Brake caliper installation; 18. Guide post; 19. Height sensor; 20. Rubber limit block; 21. Variable throttle valve; 22. Compressed air hose; 23. Auxiliary chamber.

As shown in Fig. 14, in the process of suspension vibration reduction, the vibration caused by the road surface is first transmitted to the tire assembly, and then transmitted to the motor protection shell welding body by the tire assembly, and then reaches the vertical shaft. Under the guidance of the inner sleeve of the frame connection assembly, the vertical shaft passes the vibration transmitted by the motor protection shell welding through the spring bottom support welding body, air spring, guide column, spring top support welding, steering arm welding body, positioning ring and frame connection assembly, and finally passes it to the body. Compared with the existing sprayer suspension system, the independent vertical shaft air suspension designed in this paper has the following advantages:

(1) The structure is simple and easy to process. The adjustment of the ground clearance of the sprayer can be realized by replacing the vertical shaft with different lengths. The main structural components such as motor protection shell, steering arm, steering cylinder support arm and frame connection device are welded by welding process, which reduces the manufacturing cost.

(2) The air suspension adopts the active independent suspension structure, so that the suspension can adjust the air volume in the air spring according to the different working conditions of the sprayer to achieve the best vibration reduction performance.

(3) Through the damping adjustment device composed of additional air chamber, variable throttle valve and additional air chamber, the suspension damping can be automatically adjusted according to the driving condition of the sprayer, so as to absorb the impact load transmitted from the ground to the body more effectively and ensure the ride comfort of the driver. In addition, the additional air chamber is arranged flexibly and is not limited by the suspension structure and space.

The suspension system designed in Fig. 14 is assembled on the sprayer to obtain a large high clearance self-propelled sprayer layout as shown in Fig. 15.

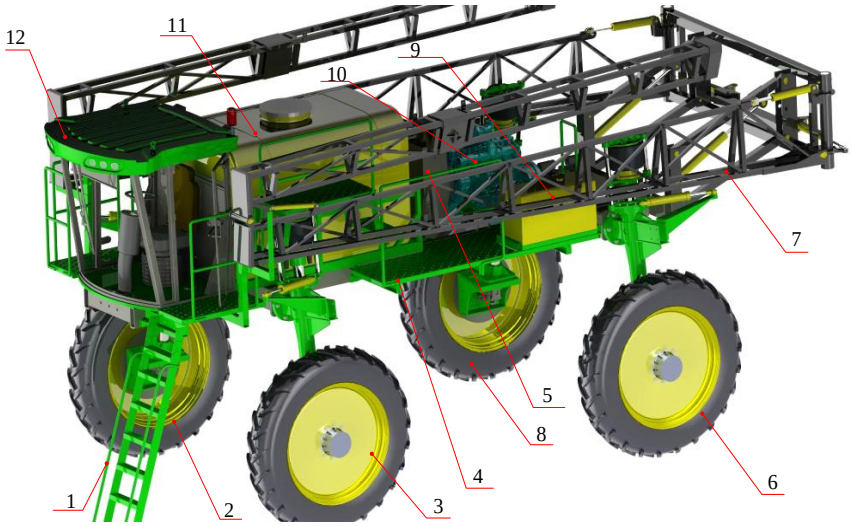

Fig. 15 – Overall structure and layout of sprayer

1. Ladder; 2. Right front suspension system; 3. Front left suspension system; 4. Walkways and handrails; 5. Radiator; 6. Rear left suspension system; 7. Spray boom; 8. Right rear suspension system; 9. Fuel tank; 10. Engine; 11. Medicine tank; 12. Cab

CONCLUSIONS

(1) According to the operating conditions and operating characteristics of the sprayer, the basic requirements of the sprayer suspension design are proposed. On this basis, the basic structural components of the suspension system, including elastic components, buffer devices, guiding devices and damping components, are analyzed and selected. A scheme of independent vertical shaft air suspension system based on air damping for high clearance sprayer is designed.

(2) Aiming at the complex mechanical action of vertical, longitudinal and lateral during the operation of the sprayer, the stress analysis of different extreme working conditions such as sideslip, emergency braking and uneven road driving of the sprayer is carried out. It is concluded that the force of the chassis is closely related to the size of the wheel track, and increasing the wheel track can reduce the force of some parts. The vertical shaft is analyzed and checked in detail, and the diameter of the vertical shaft is determined to be 120 mm. According to the relationship between the force and the reaction force, the force of the motor protection shell is calculated to be 85750 N. The force on the bottom of the steering arm is 34300 N, and the thrust of the steering cylinder is 40004 N. The reaction force of the spring top support is 57291N.

(3) According to the results of mechanical analysis, the finite element analysis of the main components of the suspension is carried out by using HyperMesh 10.0 software. Based on the analysis results, the final suspension structure is determined. The simulation results show that the size of the improved parts is consistent with the size of the mechanical check, indicating the validity of the mechanical analysis and the accuracy of the simulation structure.

ACKNOWLEDGMENT

This research was funded by the National Natural Science Foundation of China (32001428), the Key R&D projects in Shaanxi Province (2022NY-205) and the Shaanxi Provincial Key Industry Innovation Chain (Cluster) Project (2023-DLNY-62).

REFERENCES

[1] Blaauw D. (1999). *Spring-mounted spreading device*. EP, 0919124 A1[P], 1999-06-02.

[2] Buschena J. (2012). *Combination drive and suspension system for a vehicle*. US, 8172032[P], 2012-05-08.

[3] Carlson B C, Young D E, Baxter G E, et al. (2011). *Suspended axle for sprayer*. US, 7938415[P], 2011-05-10.

[4] Chen Y., Chen J., Li W., Zhang S., Xia H., Zhu Y., Wang J., (2020), Research on design and hybrid sliding mode control of high clearance self-propelled sprayer chassis air suspension, *INMATEH-Agriculture engineering*, vol.61, pp. 115-126. DOI: https://doi.org/10.35633/inmateh-61-13

[5] Chen Y., Wu J., Zhang S., Chen J., Xia H., Zhu Y., Wang J., (2021), Auto load-leveling control of a large sprayer chassis using the sliding mode method, *INMATEH-Agriculture engineering*, vol.64, pp. 65-80. DOI: https://doi.org/10.35633/inmateh-64-06

[6] Chen, Y., Mao, E., Li, W., Zhang, S., Song, Z., Yang, S., Chen, J. (2020). Design and experiment of a high-clearance self-propelled sprayer chassis. *Int J Agric & Biol Eng*, 13(2): 71-80.

[7] Chen, Y., Zhang, S., Mao, E., Du, Y., Chen, J., Yang, S. (2020). Height stability control of a large sprayer body based on air suspension using the sliding mode approach. *Information Processing in Agriculture*, 7: 20-29.

[8] Ehlen V., Voth R. (2011). *Suspension for self-propelled spreading machine*. EP, 2388157 A1[P].

[9] Giuseppe Quaglia, Massimo Sorli. Air Suspension Dimensionless Analysis and Design Procedure[J]. Vehicle System Dynamics: *International Journal of Vehicle Mechanics & Mobility*, 2001, 35(6): 443~475.

[10] Han, J.H; Park, C.H.; Jang, Y.Y. (2022). Development of a Moving Baseline RTK/Motion Sensor-Integrated Positioning-Based Autonomous Driving Algorithm for a Speed Sprayer. *Sensors,* 22, 9881.

[11] Hiddema J. (2013). Agricultural application machine with variable width track. US, 8376078 B2[P], 2013-02-19.

[12] Hu Y, Yang H, Hou B, et al. (2022). Influence of Spray Control Parameters on the Performance of an Air-Blast Sprayer[J]. *Agriculture*, 12(8): 1260.

[13] Hung T.M. (2022). Optimal selection for an air suspension system on buses through a unique high level parameter in genetic algorithms[J]. *Heliyon*, 8(3): e09059.

[14] Jiang X., Xu X., Shan H. (2022). Model-Based Fault Diagnosis of Actuators in Electronically Controlled Air Suspension System[J]. *World Electric Vehicle Journal*, 13(11): 219.

[15] Li W., Yang F., Mao E. et al. (2022). Design and Verification of Crab Steering System for High Clearance Self-Propelled Sprayer[J]. *Agriculture*, 12(11): 1893.

[16] Li W., Chen Y., Zhang S., Mao E., Du Y., Wen H. (2018). Damping Characteristic Analysis and Experiment of Air Suspension with Auxiliary Chamber. *IFAC-PapersOnLine*, 51(17): 166-172.

[17] Press R U. Raised axle and suspension system. US, 8162335 B1[P], 2012-04-24.

[18] Rondelli, V.; Capacci, E.; Franceschetti, B. (2022). Evaluation of the Stability Behavior of an Agricultural Unmanned Ground Vehicle. *Sustainability,* 14, 15561.

[19] Sánchez-Hermosilla J., Pérez-Alonso J., Martínez-Carricondo P. et al. (2022). Evaluation of Electrostatic Spraying Equipment in a Greenhouse Pepper Crop[J]. *Horticulturae*, 8(6): 541.

[20] Schaffer J A. (2002). Steering system for variable height agricultural sprayer. US, 6371237 B1[P].2002-04-16.

[21] Schaffer J A. (2002). Wheel support system for agricultural sprayer. US, 6491306 B2[P], 2002-12-10.

[22] Slawson J. (2002). Independent strut suspension. US, 8534686[P], 2013-09-17.

[23] Steffensen C., Michels E., Kleven J.E. (2012). Suspension assemblies with bump steer control, US, 8136824[P], 2012-03-20.

[24] Wei Z., Xue X., Salcedo R., Zhang Z., Gil E., Sun Y., Li Q., Shen J., He Q., Dou Q., Zhang Y. (2023). Key Technologies for an Orchard Variable-Rate Sprayer: Current Status and Future Prospects. *Agronomy,* 13, 59.

[25] Wubben T.M., Maiwald M.A., Carlson B.C. et al. (2007). High clearance vehicle suspension with twin spindles for transferring steering torque. US, 7168717 B2[P], 2007-01-30.

[26] Yu Chen, Jun Chen, Wei Li, et al. (2020). Research on design and hybrid sliding mode control of high clearance self-propelled sprayer chassis air suspension[J]. *INMATEH-Agricultural Engineering,* 61(2):115-126.

[27] Zatrieb J., Kasler R. (2012). New generation of hydro-pneumatic suspension systems with adaptive damping[R], *SAE Technical Paper*,
[28] Zheng Y., Shangguan W.B., Rakheja S. (2022), Modeling and analysis of time-domain nonlinear characteristics of air spring with an auxiliary chamber[J]. *Mechanical Systems and Signal Processing*, 176: 109161.
[29] Zheng Y., Shangguan W.B. (2023). A combined analytical model for orifice-type and pipe-type air springs with auxiliary chambers in dynamic characteristic prediction[J]. *Mechanical Systems and Signal Processing*, 185: 109830.
[30] Zhou Y., Li Z., Yu W. et al. (2022), Cooperative Control of Interconnected Air Suspension Based on Model Predictive Control[J]. *Applied Sciences*, 12(19): 9886.